RSC Advances

PAPER

View Article Online
View Journal | View Issue



Cite this: *RSC Adv.*, 2016, **6**, 78477



# Synthesis, characterization, and air stability study of pyrimido[4,5-*g*]quinazoline-4,9-dione-based polymers for organic thin film transistors†

Jesse Quinn, Yinghui He, Daid A. Khan, Jonathan Rasmussen, Haritosh Patel, Fezza Haider, Wasim Kapadia and Yuning Li*

Received 11th July 2016
Accepted 12th August 2016

DOI: 10.1039/c6ra17595c

www.rsc.org/advances

We report two novel π-conjugated polymers, **PPQ2T-TVT-24** and **PPQ2T-TT-24**, containing the pyrimido[4,5-*g*]quinazoline-4,9-dione moiety and thieno[3,2-*b*]thiophene (TT) and (*E*)-1,2-bis(thiophen-2-yl)ethene (TVT), respectively, *via* the Stille cross-coupling reaction. Both polymers displayed good thermal stability and promising field effect transistor performance with hole mobilities of up to 3.08 × $10^{-3}$ $cm^2$ $V^{-1}$ $s^{-1}$ for **PPQ2T-TT-24** and 5.34 × $10^{-3}$ $cm^2$ $V^{-1}$ $s^{-1}$ for **PPQ2T-TVT-24**. The ambient air stability of the organic thin film transistors based on these two polymers along with another previously reported PQ polymer containing bithiophene (BT) units, **PPQ2T-BT-24**, was studied. It was found that the moisture ($H_2O$) in the ambient air is a detrimental component responsible for the degradation of the device performance, while oxygen, in contrast, could enhance the carrier mobility. Our study showed that the electron donor comonomer unit significantly influenced the stability of these polymers towards moisture in the stability order of TT > BT ≫ TVT. It was shown that the interaction between $H_2O$ and **PPQ2T-TT-24** is physisorption and the device performance could be fully recovered, while the interaction of $H_2O$ with two other polymers involved chemical reactions, leading to permanent damages to the polymers and only partially recovered device performance upon removal of moisture.

## Introduction

Semiconducting polymers have been studied for over three decades in devices such as light emitting diodes, photovoltaic cells, and thin-film transistors. The strong interest to integrate polymer semiconductors in these devices originates from their attractive processing ability, diverse substrate compatibilities, versatile structural tunability, and low device fabrication costs.[1–6] Great effort has been made to develop new polymer semiconductors for organic thin film transistors (OTFTs) in order to improve their overall performance, especially charge carrier mobility and air stability,[7–12] two performance parameters that are key for many applications. Among the high performance polymers reported for OTFTs, the ones comprised of amide/imide containing building blocks[13] are of particular interest and most widely studied recently due to several reasons: (a) the strong electron withdrawing amide/imide group can lower the lowest unoccupied molecular orbital (LUMO) energy level of the polymer to stabilize electron transport; (b) the amide/imide building blocks can also lower the highest occupied molecular orbital (HOMO) level to stabilize the hole transport; (c) the *N*-alkylation of amide/imide groups provides a tool to render the polymer solution processable; (d) the *N*-alkyl chains are usually distant from aromatic cores, minimizing the steric hindrance to maintain coplanarity of the polymer backbone for efficient intramolecular charge transport.

Recently, we reported a new amide containing building block, pyrimido[4,5-*g*]quinazoline-4,9-dione (PQ),[14,15] for polymer semiconductors. Our research into PQ polymers is driven by the known bioactivities of PQ derivatives that have been studied as anti-microbial, anti-tumour, anti-inflammatory, anti-convulsant, anti-hypertensive, and anti-

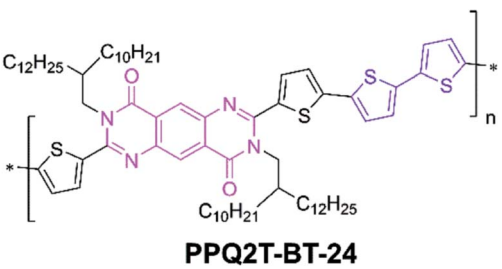


**PPQ2T-BT-24**

Fig. 1 Structure of **PPQ2T-BT-24**.[14]

*Department of Chemical Engineering, Waterloo Institute of Nanotechnology, (WIN), University of Waterloo, 200 University Ave West, Waterloo, Ontario, N2L 3G1, Canada. E-mail: yuning.li@uwaterloo.ca; Fax: +1-519-888-4347; Tel: +1-519-888-4567 ext. 31105*

† Electronic supplementary information (ESI) available: Details of computer simulations, TGA, DSC, and additional OTFT data. See DOI: 10.1039/c6ra17595c

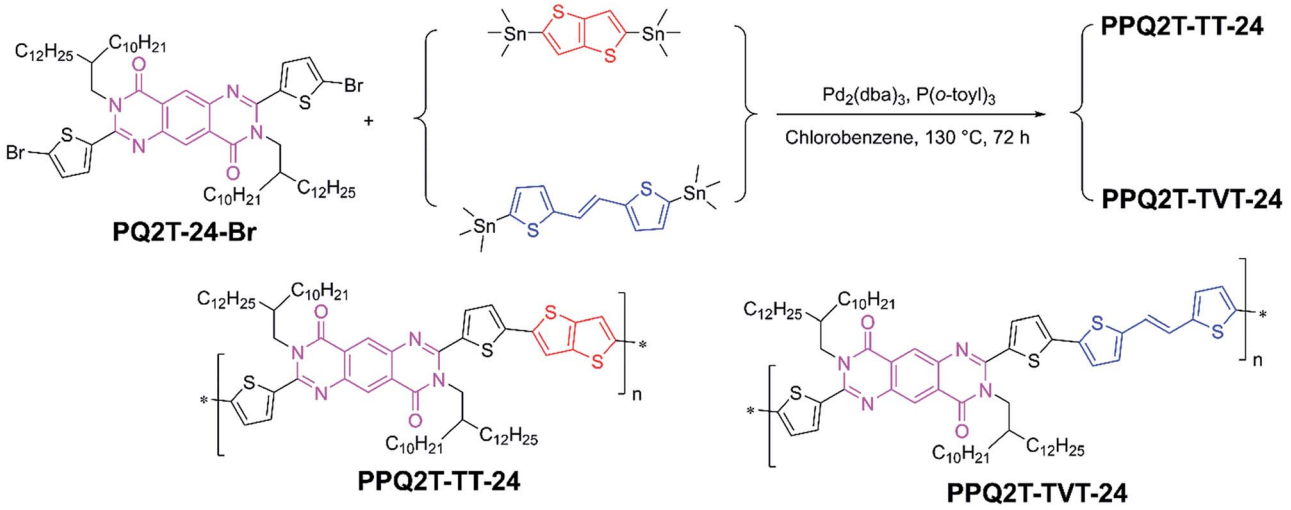


Scheme 1 Synthetic route to PPQ2T-TT-24 and PPQ2T-TVT-24.

malarial agents.[16–23] Our previous results showed that the copolymers of PQ and bithiophene (**PPQ2T-BT-24** shown in Fig. 1 and **PPQ2T-BT-40**) are highly sensitive to acids, which can potentially be used as active channel layers in OTFT based bio- and chemo-sensors.[14] These two polymers demonstrated modest charge carrier performance ($\sim 10^{-3}$ $cm^2 V^{-1} s^{-1}$) in OTFTs. It is known that the comonomer to the amide/imide-containing monomer is critical for charge transport performance. For example, for DPP-based polymers, the charge carrier mobility values vary from $\sim 10^{-3}$ $cm^2 V^{-1} s^{-1}$ to 17.8 $cm^2 V^{-1} s^{-1}$ depending on the chosen comonomer unit, which can regulate the frontier molecular orbital energy levels, molecular packing, and thin-film morphology.[24–28] Thieno[3,2-*b*]thiophene (TT) and (*E*)-1,2-bis(thiophen-2-yl)ethene (TVT) have been used as donor building blocks to couple with the electron-withdrawing amide/imide building blocks forming donor–acceptor (D–A) polymers that exhibit very high charge carrier mobility values,[29–31] sometimes greater than those of BT-containing polymers. To further explore the potential of PQ as a building block in polymer semiconductors, in this work, we selected these two comonomer units to make two novel PQ-based π-conjugated polymers, **PPQ2T-TT-24** and **PPQ2T-TVT-24**, respectively (Scheme 1). When used as active channel layers in OTFTs, **PPQ2T-TT-24** and **PPQ2T-TVT-24** demonstrated charge carrier mobilities of $\sim 10^{-3}$ $cm^2 V^{-1} s^{-1}$ that are similar to that of **PPQ2T-BT-24** under nitrogen atmosphere. When the devices were operated in the ambient air (with 52% relative humidity, RH), **PPQ2T-TT-24** exhibited better stability than **PPQ2T-TVT-24** and **PPQ2T-BT-24**. To decouple the influences of air and moisture ($H_2O$) in the ambient air on device performance, three PQ polymers were tested under dry air and moist nitrogen atmospheres. It was shown that moisture in the air has a detrimental effect on the hole mobility with differing mechanisms for three polymers. Surprisingly, the dry air (or oxygen) improved the hole mobility of these polymers.

## Results and discussion

Fig. 2 shows the optimized geometry at ground state with LUMO and HOMO wavefunctions for PQ2T-TT-Me and PQ2T-TVT-Me dimers, respectively, obtained by density functional theory (DFT) at the B3LYP 6-31G(d) level of theory. As observed in our previous findings,[14] the dihedral angle between the PQ moiety and the flanking thiophene unit is ~26°, which is considered a limiting factor for achieving a high coplanarity (ESI†). The calculated frontier energy levels, LUMO/HOMO, for PQ2T-TT-Me and PQ2T-TVT-Me dimers are −2.57 eV/−5.26 eV and −2.62 eV/−5.04 eV, respectively. The LUMO wavefunction localizes at TT (or TVT) and the flanking thiophene units and thus give relatively high LUMO energy levels, whereas the HOMO wavefunction is delocalized along the dimer backbones across the PQ and TT (or TVT) units. In comparison with the LUMO/HOMO of PQ2T-BT-Me (−2.57 eV/−5.17 eV),[14] it appears that the HOMO levels changed notably with differing donor comonomer units (HOMO: TT < BT < TVT), while their LUMO levels remain similar.

Polymers **PPQ2T-TT-24** and **PPQ2T-TVT-24** were synthesized *via* Stille coupling polymerization of 2,7-bis(5-bromothiophen-2-yl)-3,8-bis(2-decyltetradecyl)-3,8-dihydropyrimido[4,5-*g*]quinazoline-4,9-dione[15] with 2,5-bis(trimethylstannyl)thieno[3,2-*b*]thiophene and 1,2-bis(5-(trimethylstannyl)thiophen-2-yl)ethene, respectively (Scheme 1). The polymers were purified using Soxhlet extraction sequentially with acetone, hexanes, and chloroform. The chloroform fraction was then concentrated by removing some solvent and precipitated from methanol. After drying, **PPQ2T-TT-24** and **PPQ2T-TVT-24** were obtained in 82% and 87% yields, respectively. The number average molecular weight ($M_n$) and polydispersity index (PDI) were measured to be 18.3 kg $mol^{-1}$ and 2.23 for **PPQ2T-TT-24** and 19.4 kg $mol^{-1}$ and 2.52 for **PPQ2T-TVT-24**, respectively (ESI†). Data were obtained using high-temperature gel-permeation chromatography (HT-GPC) at 140 °C with 1,2,4-trichlorobenzene as an eluent and polystyrene as the standards.

 

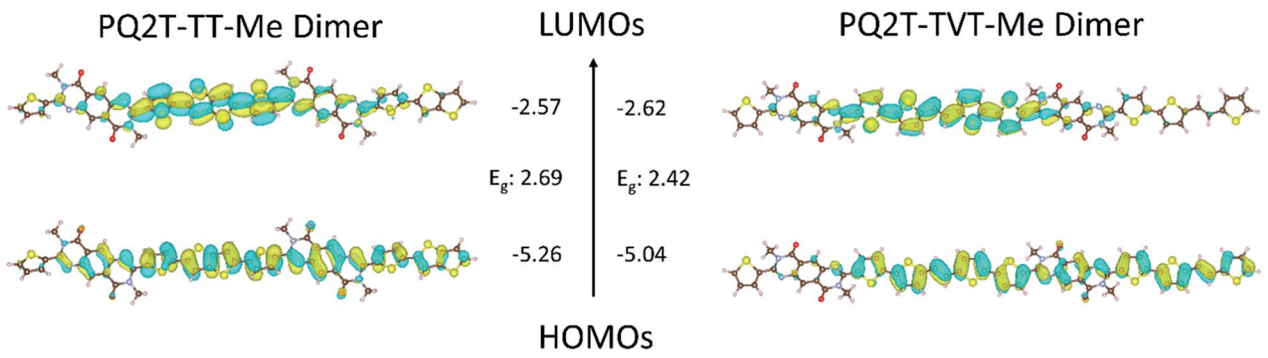


Fig. 2 Orbital density distribution (wavefunctions) for the frontier molecular orbitals of PQ2T-TT-Me and PQ2T-TVT-Me dimers. DFT calculations were performed using the Gaussian 09 suite of programs and the B3LYP/6-31G(d) level of theory.[32] Theoretical HOMO/LUMO energy levels and band-gaps (*vs.* vacuum scale) are also shown.

The thermal properties of the polymers were characterized by thermogravimetric analysis (TGA) and differential scanning calorimetry (DSC) (ESI†). **PPQ2T-TT-24** and **PPQ2T-TVT-24** showed 5% weight loss temperatures ($T_{-5\%}$) of 366 °C and 376 °C, respectively, on their TGA thermograms. Both polymers showed visible glass transition temperatures at ~60–70 °C on their DSC thermograms.

To elucidate the polymer chain ordering, XRD measurements were performed with polymer thin films spin coated on a DDTS-modified $SiO_2$/Si wafer and annealed at different temperatures (Fig. 3). At an annealing temperature of 80 °C, a primary (100) diffraction peak at $2\theta = 4.03°$, which corresponds to a *d*-spacing distance of 2.19 nm, and a low intensity secondary (200) diffraction peak ($2\theta = 8.22°$) were observed for **PPQ2T-TT-24**. A slight increase in the intensity for the (100) and (200) peaks occurred at an annealing temperature of 100 °C, whereas further increasing the annealing temperature results in a gradual increase in the intensity of the (100) and (200) peaks. At an annealing temperature of 250 °C and above, a decrease in the peak intensity was observed. Since the TGA data show that these polymers should be stable at 250 and 300 °C and the UV-vis spectra of the films showed no significant changes in the 250 °C- and 300 °C-annealed films compared with films annealed at lower temperatures (see Fig. S9 in the ESI†), this reduction of the peak intensity might be caused by the creation of pin-holes at these high temperatures (see the AFM images in Fig. 5), which reduced the coverage of the substrate by the polymer film. For the **PPQ2T-TVT-24** thin film annealed at 80 °C, a weak (100) peak at $2\theta = 4.39°$ (*d*-spacing = 2.01 nm) appeared. With increasing annealing temperature, the intensity of the (100) peak grew, along with the appearance of a secondary (200) diffraction peak ($2\theta = 8.58°$). For the 250 °C- and 300 °C-annealed films, a reduction in the peak intensity was also observed due probably to the formation of pin-holes discussed as above for **PPQ2T-TT-24**.

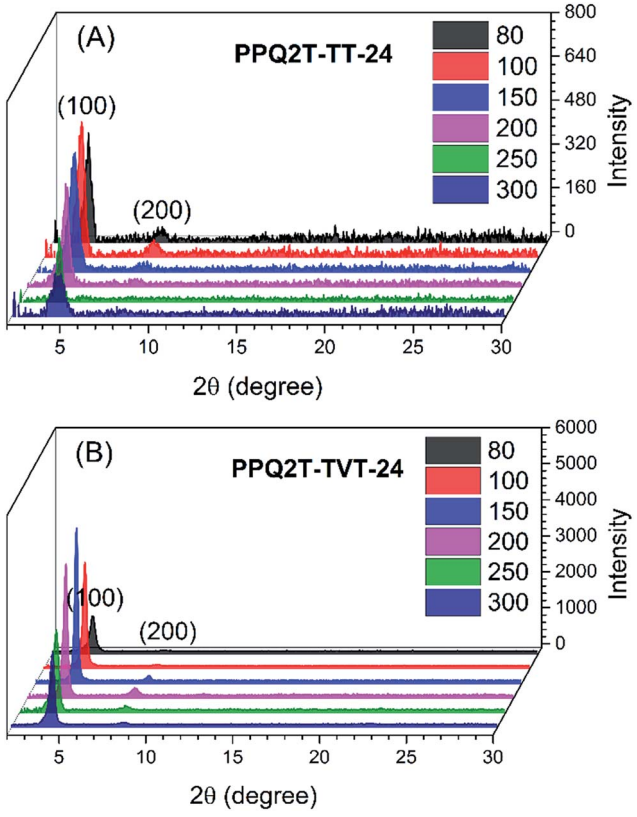


Fig. 3 XRD patterns of PPQ2T-TT-24 (A) and PPQ2T-TVT-24 (B) thin films after annealing in nitrogen at different temperatures, respectively.

The UV-vis absorption spectra of **PPQ2T-TT-24** and **PPQ2T-TVT-24** in chloroform and in thin films are shown in Fig. 4. **PPQ2T-TT-24** showed a wavelength of maximum absorption ($\lambda_{max}$) at 522 nm (along with a shoulder at ~548 nm) for solution and 521 nm (along with a shoulder at ~556 nm) for the thin film. **PPQ2T-TVT-24** showed a similar absorption pattern with the $\lambda_{max}$ at 537 nm (along with a shoulder at ~571 nm) in solution and 536 nm (along with a shoulder at ~575 nm) for the thin-film. The more resolvable vibronic splitting or the more pronounced absorption shoulders at the long wavelength side of the spectra of the thin film compared to the solution spectra are characteristic of more ordered polymer chains in the solid state[33–35] and were observed for our previously reported PQ-based polymer **PPQ2T-BT-24**.[14] The optical band gaps ($E_g^{opt}$) were calculated from the UV-vis absorption spectra edge

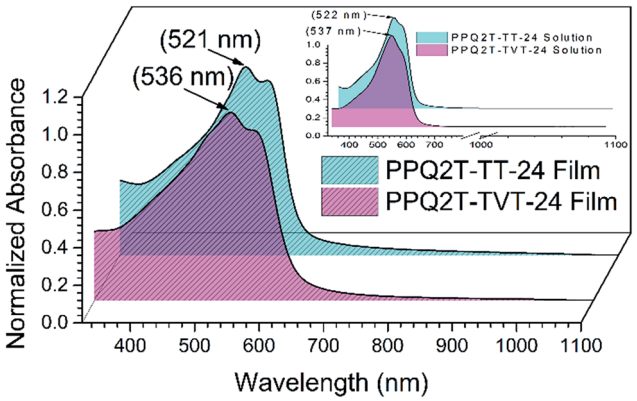


Fig. 4 UV-vis absorption spectra of PPQ2T-TT-24 and PPQ2T-TVT-24 as thin films and in chloroform solution (inset).

and found to equal 2.0 eV and 1.9 eV for **PPQ2T-TT-24** and **PPQ2T-TVT-24**, respectively, which are similar to the $E_g^{opt}$ of **PPQ2T-BT-24** (2.0 eV). The experimental $E_g^{opt}$ is in good agreement with the expected trend observed in the computational study. UV-vis spectra of the films of these two polymers annealed at temperatures up to 300 °C showed no noticeable changes, indicating their excellent thermal stability (Fig. S9†).

The morphological changes of the polymer thin films were examined by atomic force microscopy (AFM) (Fig. 5). The **PPQ2T-TT-24** film annealed at temperatures lower than 200 °C showed large particles (irregular shaped bright spots) of a few hundred nanometers in size. The formation of large particles might be due to the poor solubility of this polymer that caused precipitation of polymer aggregates as solvent evaporated during spin coating. As the annealing temperature was increased to 250 °C, these particles disappeared accompanied with the formation of pin-holes (dark spots). The number of pin-holes increased as the annealing temperature was increased to 300 °C. The formation of pin-holes is likely due to the weakened interfacial interaction between the polymer film and the substrate at high temperatures. The 80 °C-annealed **PPQ2T-TVT-24** film showed some round-shaped particles (bright spots) and well-defined grains. Similar to **PPQ2T-TT-24**, the number of (bright) particles decreases with increasing annealing temperature. The particles almost disappeared at the annealing temperature of 200 °C, 50 °C lower compared with **PPQ2T-TT-24**. However, pin-holes also starts to appear at 200 °C, indicating that the interfacial interaction between the **PPQ2T-TVT-24** film and the substrate is weaker than that between **PPQ2T-TVT-24** and the substrate.

Cyclic voltammetry (CV) measurements were conducted on the polymer thin-films (ESI†) using ferrocene as a reference with a reported HOMO energy level of −4.8 eV against vacuum.[36] The HOMO energy levels are thus calculated to be −5.42 eV and −5.18 eV for **PPQ2T-TT-24** and **PPQ2T-TVT-24**, falling below and above that of **PPQ2T-BT-24** (−5.30 eV), respectively, which are also in good agreement with the trend observed in the computational study. It should be noted that most of the p-type polymer semiconductors with high hole mobility have a relatively high HOMO level between −5.1 eV and −5.3 eV.[30,37,38] Therefore, the HOMO level of **PPQ2T-TVT-24** should be more favoured for hole injection and transport. No peaks were observed during the reduction cycles, so the LUMO levels were calculated from the HOMO levels and $E_g^{opt}$ to be −3.41 eV and −3.27 eV for **PPQ2T-TT-24** and **PPQ2T-TVT-24** respectively.

A bottom-gate bottom-contact (BGBC) transistor architecture was used to evaluate the charge carrier transport characteristics for each polymer. $n^{++}$-Doped conductive silicon wafer with a $SiO_2$ dielectric layer (~300 nm thick) was used as the substrate. Both polymers only showed hole transport performance due to their relatively high LUMO levels. A LUMO level of ~−3.7 eV to ~−4.0 eV or deeper is required for stable n-type performance.[39–41] **PPQ2T-TT-24** devices showed the best performance with the 300 °C-annealed films reaching a maximum hole mobility of $3.08 \times 10^{-3}$ $cm^2$ $V^{-1}$ $s^{-1}$ (Fig. 6A) and an average mobility of $2.33 \times 10^{-3}$ $cm^2$ $V^{-1}$ $s^{-1}$ (Table S1†). **PPQ2T-TVT-24** devices performed the best for the 150 °C-annealed films reaching a maximum hole mobility of $5.34 \times 10^{-3}$ $cm^2$ $V^{-1}$ $s^{-1}$ (Fig. 6B) and an average mobility of $4.81 \times 10^{-3}$ $cm^2$ $V^{-1}$ $s^{-1}$ (Table S1 in the ESI†). At an annealing temperature greater than 200 °C, the mobility values dropped. This mobility reduction trend coincidently agrees with the formation of pin-holes as observed in the AFM images (Fig. 5). These pin-holes

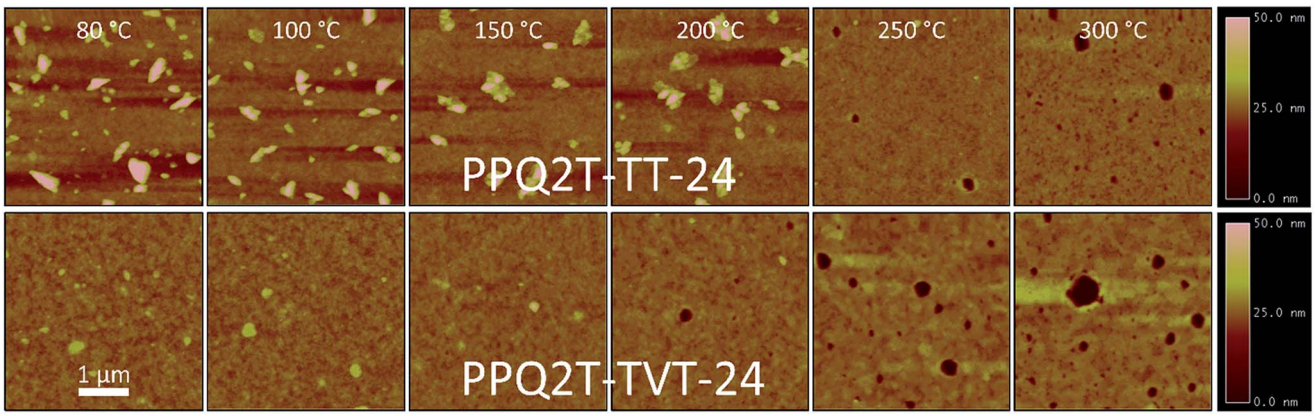


Fig. 5 AFM images (4 μm × 4 μm) of PPQ2T-TT-24 and PPQ2T-TVT-24 thin films after annealing at desired temperatures.

 

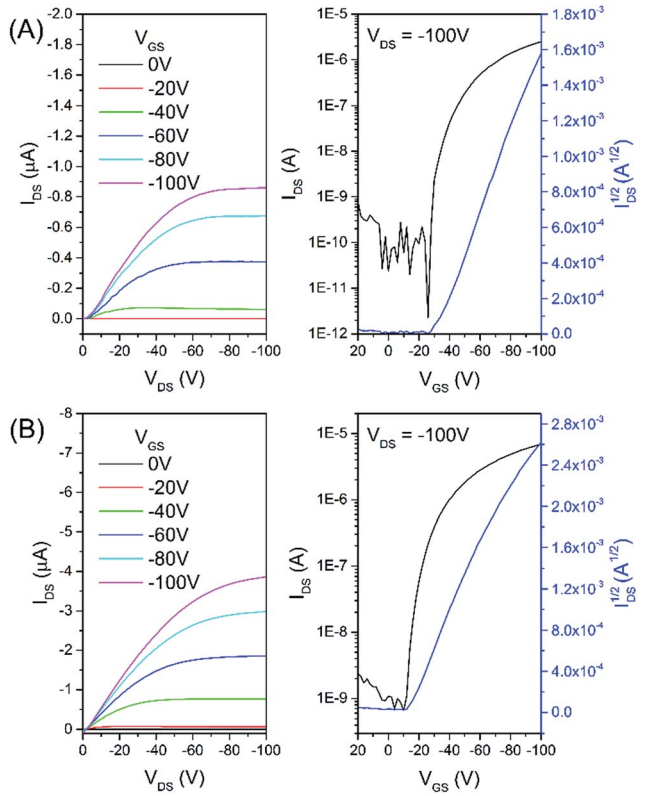


Fig. 6 Output (left) and transfer (right) curves for OTFT devices using **PPQ2T-TT-24** (A) and **PPQ2T-TVT-24** (B) under nitrogen annealed at 300 °C and annealed at 150 °C, respectively.

would interrupt the charge transport pathways. As aforementioned, the formation of pin-holes is due to the weakened polymer–substrate interface, which would also negatively influence the charge carrier mobility due to the poorer polymer–dielectric contact.[42–44]

The devices using polymer films annealed at 200 °C were subject to testing in the ambient air (with 52% RH) after testing in dry nitrogen in a glove box. The **PPQ2T-TT-24** based devices measured in the ambient air showed a decrease of 18% in the average mobility with respect to that measured in dry nitrogen (Fig. 7A). On the other hand, the mobility of the **PPQ2T-TVT-24** based devices dropped almost completely (~94%) upon exposing to the ambient air. We also tested the air stability of devices with the previously reported polymer **PPQ2T-BT-24**, which showed a decrease of ~49% in mobility compared with the value measured in dry nitrogen.

These devices were then moved back to the nitrogen-filled glove box, baked at 100 °C for 1 h to remove adsorbed moisture and oxygen, and tested again. The average mobility of the **PPQ2T-BT-24** based devices recovered by 70% of the value initially measured in the glove box in dry nitrogen (Fig. 7A). The **PPQ2T-TVT-24** based devices showed negligible field effect performance, indicating that once these devices were measured in the ambient air, they underwent permanent damages. Interestingly, the **PPQ2T-TT-24** based devices exhibited a 17% increase in the average mobility compared to that obtained

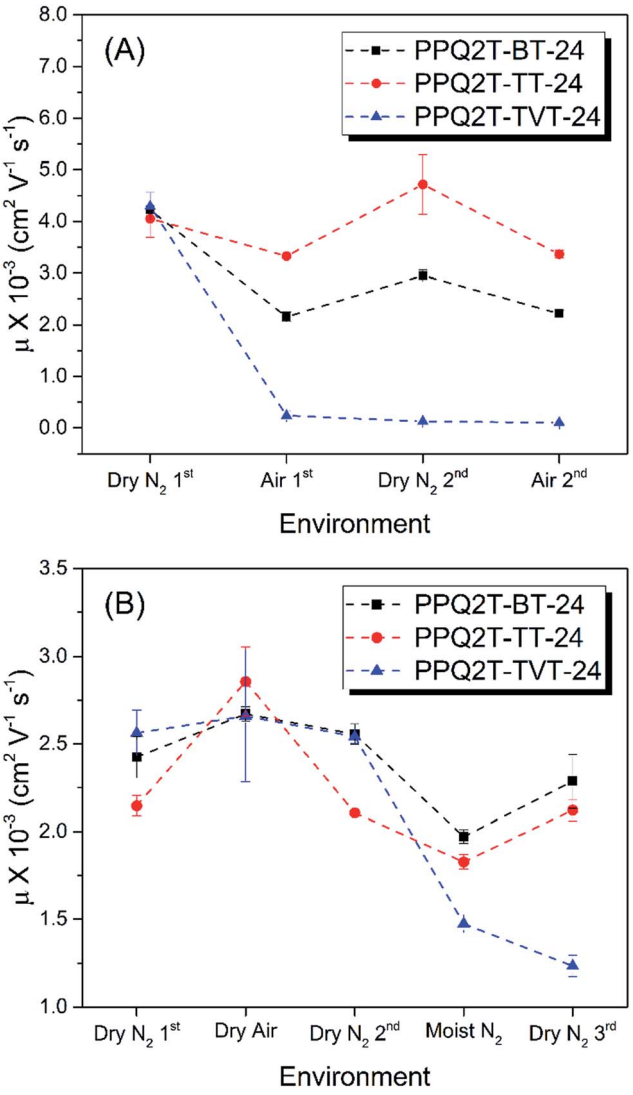


Fig. 7 Hole mobility comparison for OTFT devices using different polymers in nitrogen and subsequently in air (~52% relative humidity) consecutively (A) and under specific environments (B). See ESI† for voltage threshold comparisons.

initially in dry nitrogen. It has been reported that numerous factors might influence the ambient stability of OTFT materials/devices,[45–47] which is still a subject of intense research.[48–51] As reported by Lu *et al.*,[52] the ambient stability of polymer semiconductors in regard to oxidative doping is governed by the ionization potential or the HOMO energy level of the polymers. This is evident by the trend observed in this study (Fig. 7A) where **PPQ2T-TT-24** with the deepest HOMO level of −5.42 eV shows the greatest stability, while **PPQ2T-TVT-24** with the highest HOMO level of −5.18 eV shows the poorest stability in the ambient air. Since air is composed of nitrogen, oxygen, water vapour, and small amounts of other gases, it is reasonable to assume that oxygen and moisture ($H_2O$) are the two major components that may degrade the device performance of these polymers. It has been reported that dry oxygen had little effect on the field effect characteristics[54] or some enhancement effects

on the saturation current and mobility[55] of pentacene based OTFTs. It was also found that the absorbed $H_2O$ at the grain boundaries of the pentacene film could either decrease the mobility by trapping charge carriers and altering the film morphology[53,54] or increase the mobility by forming water clusters.[54,55] To gain a better understanding of the influences of air (free of moisture) and moisture (free of oxygen) separately on the performance of our polymers, devices were characterized sequentially under dry nitrogen (in a glove box), dry air (in a container filled with dry air), dry nitrogen (in the same glove box), moist nitrogen (in a container filled with nitrogen saturated with water vapor), and finally in dry nitrogen (in a glove box) (Fig. 7B). For all three polymers, their devices showed increased hole mobilities in dry air with the largest increase by ~33% observed for **PPQ2T-TT-24**, indicating dry oxygen is not harmful but beneficial for the hole transport, which agrees with the observation in a report on pentacene OTFTs.[55] This enhancement in hole mobility, which was also observed for another p-type polymer reported by our group,[51] can be interpreted by the increased work function by oxygen.[24] For the pentacene devices, the increases in the saturation current and mobility were attributed to the formation of a charge transfer complex (or p-doping) between pentacene and $O_2$.[55] However, it is unlikely the case for our polymers, because **PPQ2T-TT-24**, which has the deepest HOMO level, or is the most difficult to be p-doped by $O_2$, showed the largest enhancement in mobility among three polymers (Fig. 7B).

Once the devices were returned to the glove box for re-testing under dry nitrogen, the mobilities dropped to similar levels obtained in the first measurement in dry nitrogen. This further demonstrated that dry oxygen did not damage the polymers. Once the devices were taken to the moist nitrogen atmosphere and tested, the mobilities of **PPQ2T-TT-24** and **PPQ2T-BT-24** dropped by 15% and 19%, respectively. The **PPQ2T-TVT-24** devices showed the largest drop in mobility by 43%. To examine if the effect of moisture on the device performance is reversible, the devices were measured in the $N_2$-filled glove box again (for the 3$^{rd}$ time). It was shown that the average mobility of the **PPQ2T-TT-24** based devices fully recovered to the value obtained in the first and second measurements in dry $N_2$ (Fig. 7B). On the other hand, the **PPQ2T-BT-24** and **PPQ2T-TVT-24** based devices partially recovered by ~90% and ~50% of the mobilities obtained before exposing to the moist $N_2$, respectively, indicating that part of the performance degradation in moist nitrogen is permanent for these two polymers. These results manifest that water, not oxygen, in the ambient air has a detrimental effect on the hole transport performance of these polymers. Our study also showed that different donor comonomers have dramatic influences on the ambient air stability or more precisely the stability towards $H_2O$. The TT-containing polymer, **PPQ2T-TT-24**, showed the best stability in the ambient air and the device performance can be recovered once the devices were returned to a dry nitrogen atmosphere, which indicates that the drop in mobility for this polymer is mainly caused by physisorption of water molecules that might function as hole traps. On the other hand, **PPQ2T-BT-24** and **PPQ2T-TVT-24**, in particular, undergo chemical reactions with water, causing permanent damages to the polymers and the device performance cannot be fully recovered. Since these polymers are stable when stored in the ambient air, the chemical reactions of these polymers with water presumably occur under a positively charged state during the device operation in the hole accumulation mode.

# Conclusions

We report two novel π-conjugated polymers, **PPQ2T-TT-24** and **PPQ2T-TVT-24**, containing pyrimido[4,5-*g*]quinazoline-4,9-dione (PQ) and the electron donor comonomer units, thieno[3,2-*b*]thiophene (TT) and (*E*)-1,2-bis(thiophen-2-yl)ethene (TVT), respectively. The UV-vis absorption characteristics, frontier energy levels, crystallinity, as well as thin film morphology were found to vary notably with different donor units. Both polymers showed typical hole transport performance as channel semiconductors in OTFTs with mobilities as high as $3.08 \times 10^{-3}$ cm$^2$ V$^{-1}$ s$^{-1}$ for **PPQ2T-TT-24** and $5.34 \times 10^{-3}$ cm$^2$ V$^{-1}$ s$^{-1}$ for **PPQ2T-TVT-24**. Device stability of these two polymers together with another previously reported PQ polymer, **PPQ2T-TT-24**, was systematically investigated in different atmospheres: dry nitrogen, moist nitrogen, dry air, and ambient air (~52% RH). It was found that oxygen could enhance the hole mobility of these polymers, which was interpreted by the increased work function of the gold contact electrodes that facilitated hole injection. On other hand, moisture ($H_2O$) notably decreased the mobility of all three polymers. Interestingly, the device performance of **PPQ2T-TT-24** could be fully recovered, indicating the interaction between $H_2O$ and this polymer is physisorption and the decrease in mobility is due to trapping of charge carriers. For **PPQ2T-BT-24** and **PPQ2T-TVT-24**, the mobilities of their OTFT devices that were tested in the presence of moisture could only be partially recovered when measured in dry $N_2$ again, which indicates that the interaction of $H_2O$ with these two polymers involved chemical reactions leading to permanent damages of the polymer structures during device operation. Our results revealed that the electron donor comonomer in a PQ polymer and possibly in other D–A polymers has a significant effect on the ambient air stability or more precisely the stability towards the moisture, with the stability order of TT > BT ≫ TVT. Our study provided useful guidance on the design of ambient air (or moisture) stable polymer semiconductors for printed electronics by choosing appropriate donor monomer building blocks.

# Experimental

### Materials and instrumentation

Chemical reagents were purchased from Sigma Aldrich and used without further purification. 2,7-Bis(5-bromothiophen-2-yl)-3,8-bis(2-decyltetradecyl)-3,8-dihydropyrimido[4,5-*g*]quinazoline-4,9-dione (PQ2T-24-Br) was synthesized according to our previously reported method.[15] NMR data were recorded on a Bruker DPX

 

300 MHz spectrometer with chemical shifts relative to the residual $CHCl_3$ in the deuterated solvent (7.26 ppm for $CHCl_3$).[56] GPC measurements were performed on a Malvern SEC system using 1,2,4-trichlorobenzene as eluent and polystyrene as standards at 140 °C. TGA measurements were carried out on a TA Instruments Q500 at a temperature ramping rate of 10 °C $min^{-1}$ under nitrogen atmosphere. DSC measurements were carried out on a TA Instruments Q2000 at a temperature ramping rate of 20 °C $min^{-1}$ under nitrogen atmosphere. The UV-vis absorption spectra of polymers were recorded on a Thermo Scientific GENESYS™ 10S VIS spectrophotometer. Cyclic voltammetry (CV) data were obtained on a CHI600E electrochemical analyzer using an Ag/AgCl reference electrode and two platinum disk electrodes as the working and counter electrodes in a 0.1 M tetrabutylammonium hexafluorophosphate ($Bu_4NPF_6$) anhydrous acetonitrile solution at a scan rate of 50 mV $s^{-1}$. Ferrocene acted as a reference with a reported HOMO energy level of −4.8 eV.[36] Thin-film XRD diagrams of polymer thin-films (~40 nm) spin-coated on dodecyltrichlorosilane (DDTS) modified $SiO_2$/Si substrates and annealed at chosen temperatures for 20 min under nitrogen atmosphere were obtained using a Bruker D8 Advance powder diffractometer with Cu K$\alpha$1 radiation ($\lambda = 0.15406$ nm). Atomic force microscopy (AFM) images were taken on polymer thin films spin-coated on the DDTS modified $SiO_2$/Si substrates with a Dimension 3100 scanning probe microscope. Density functional theory (DFT) calculations were performed through Gaussian 09 Revision D.01 (ref. 32) using the functional B3LYP and the basis set 6-31G(d) under tight convergence to investigate the geometry, molecular energy levels, and electron distributions for the model compounds.

### Synthesis of PPQ2T-TT-24

A 25 mL dry Schlenk flask was charged with PQ2T-24-Br (0.10 g, 0.09 mmol), 2,5-bis(trimethylstannyl)thieno[3,2-*b*]thiophene (0.040 g, 0.09 mmol), and tri(*o*-tolyl)phosphine (P(*o*-tolyl)$_3$) (2 mg, 0.01 mmol). After degassing and refilling argon three times, anhydrous chlorobenzene (3 mL) and tris-(dibenzylideneacetone)-dipalladium ($Pd_2dba_3$) (2 mg, 0.002 mmol) were added under an argon atmosphere. The reaction mixture was stirred at 130 °C for 72 h. Upon cooling to room temperature, the reaction mixture was poured into methanol, and the precipitate was collected by filtration and subjected to Soxhlet extraction sequentially with acetone, hexanes, and chloroform. The chloroform solution was concentrated and precipitated in methanol. The precipitate was filtered and dried under vacuum to obtain a red-colored solid. Yield: 90 mg (82%). $^1$H-NMR spectrum is provided in ESI.† Elemental analysis: calculated for $(C_{72}H_{106}N_4O_2S_4)_n$ (%): C 72.80, H 8.99, N 4.72; S 10.80 found (%): C 71.38, H 7.97, N 4.55, S 9.74.

### Synthesis of PPQ2T-TVT-24

This polymer was synthesized and purified using a similar procedure described for the synthesis of **PPQ2T-TT-24**, except that 1,2-bis(5-(trimethylstannyl)thiophen-2-yl)ethene (0.044 g, 0.09 mmol) was used as a comonomer in replacement of 2,5-bis(trimethylstannyl)thieno[3,2-*b*]thiophene. The product is a purple-colored solid. Yield: 96 mg (87%). $^1$H-NMR spectrum is provided in ESI.† Elemental analysis: calculated for $(C_{76}H_{110}N_4O_2S_4)_n$ (%): C 73.62, H 8.94, N 4.52; S 10.34 found (%): C 72.50, H 7.93, N 4.18, S 9.63.

### OTFT device fabrication

Bottom-gate bottom-contact (BGBC) OTFT architecture was utilized for evaluating the polymers. An $n^{++}$-doped Si wafer with a 300 nm thick $SiO_2$ layer (dielectric) was used as the substrate. The gold source and drain electrodes were deposited onto the substrate by common photolithography and thermal evaporation methods. The substrate was then plasma treated and cleaned by ultra-sonication with acetone, isopropanol, and dried with nitrogen and baked at 120 °C for 1 min. The substrate was then cooled to room temperature, dried, and submerged in a DDTS solution (3% in toluene) for 20 min and then rinsed with toluene and dried with nitrogen. Polymer films with a thickness of ~40 nm were deposited on the substrate by spin-coating a polymer solution in chloroform (5 mg $mL^{-1}$) at 3000 rpm for 80 s and then annealed at an intended temperature for 20 min under nitrogen atmosphere in a glovebox. After annealing, the device performance was measured under nitrogen in the same glovebox and in the absence of light using an Agilent B2912A Precision source/measure unit. Devices characterized in the ambient air were annealed under nitrogen in the glovebox and then tested outside the glovebox in ambient room conditions with a relative humidity of 52%. Devices characterized in dry air and moist nitrogen were kept in a custom-made sealed chamber with electrical contacts for source, drain, and gate. Gases enter and leave *via* two ports. The charge carrier mobility ($\mu$) and voltage threshold ($V_{TH}$) in the saturation regime were calculated by using a slope obtained from the linear fitting of $(I_{DS})^{1/2}$ against $V_{GS}$ according to the equation:[57]

$$I_{DS} = \left(\frac{W}{2L}\right) C_i \mu (V_{GS} - V_{TH})^2$$

where $I_{DS}$ is the drain current, $C_i$ is the insulator capacitance per unit area (~11.6 nF $cm^{-2}$), and $V_{GS}$ is the gate voltage, respectively. Device dimensions were 1 mm in width ($W$) and 30 μm in length ($L$). In the case for devices characterized in dry air and moist nitrogen device dimensions were 16.25 mm in width and 30 μm in length.

## Acknowledgements

Financial support of this work by the Natural Sciences and Engineering Research Council (NSERC) of Canada (Discovery Grant # RGPIN-2016-04366) is acknowledged.

## Notes and references

1 H. Sirringhaus, N. Tessler and R. H. Friend, *Science*, 1998, **280**, 1741–1744.

2 C. D. Dimitrakopoulos and P. R. L. Malenfant, *Adv. Mater.*, 2002, **14**, 99–117.
3 S. R. Forrest, *Nature*, 2004, **428**, 911–918.
4 H. Sirringhaus, *Adv. Mater.*, 2005, **17**, 2411–2425.
5 H. Yan, Z. Chen, Y. Zheng, C. Newman, J. R. Quinn, F. Dötz, M. Kastler and A. Facchetti, *Nature*, 2009, **457**, 679–686.
6 A. Facchetti, *Chem. Mater.*, 2011, **23**, 733–758.
7 P. Sonar, S. P. Singh, Y. Li, Z.-E. Ooi, T. Ha, I. Wong, M. S. Soh and A. Dodabalapur, *Energy Environ. Sci.*, 2011, **4**, 2288–2296.
8 A. Pron and M. Leclerc, *Prog. Polym. Sci.*, 2013, **38**, 1815–1831.
9 Y. Li, P. Sonar, L. Murphy and W. Hong, *Energy Environ. Sci.*, 2013, **6**, 1684–1710.
10 X. Guo, M. Baumgarten and K. Müllen, *Prog. Polym. Sci.*, 2013, **38**, 1832–1908.
11 Y. He, W. Hong and Y. Li, *J. Mater. Chem. C*, 2014, **2**, 8651–8661.
12 C. Luo, A. K. K. Kyaw, L. A. Perez, S. Patel, M. Wang, B. Grimm, G. C. Bazan, E. J. Kramer and A. J. Heeger, *Nano Lett.*, 2014, **14**, 2764–2771.
13 X. Guo, A. Facchetti and T. J. Marks, *Chem. Rev.*, 2014, **114**, 8943–9021.
14 J. Quinn, C. Guo, B. Sun, A. Chan, Y. He, E. Jin and Y. Li, *J. Mater. Chem. C*, 2015, **3**, 11937–11944.
15 J. Quinn, E. Jin and Y. Li, *Tetrahedron Lett.*, 2015, **56**, 2280–2282.
16 M. J. Fray, J. P. Mathias, C. L. Nichols, Y. M. Po-Ba and H. Snow, *Tetrahedron Lett.*, 2006, **47**, 6365–6368.
17 U. a. Kshirsagar, S. B. Mhaske and N. P. Argade, *Tetrahedron Lett.*, 2007, **48**, 3243–3246.
18 Z. Zhang, X. Liang, X. Li, T. Song, Q. Chen and H. Sheng, *Eur. J. Med. Chem.*, 2013, **69**, 711–718.
19 S. G. Yerande, S. D. More, M. Bhandari, K. M. Newase, K. Khoury, K. Wang and A. Dömling, *J. Heterocycl. Chem.*, 2014, **51**, E358–E363.
20 M.-M. Zhang, L. Lu and X.-S. Wang, *J. Heterocycl. Chem.*, 2014, **51**, 1363–1368.
21 H. Chai, J. Li, L. Yang, H. Lu, Z. Qi and D. Shi, *RSC Adv.*, 2014, **4**, 44811–44814.
22 I. Khan, A. Ibrar, W. Ahmed and A. Saeed, *Eur. J. Med. Chem.*, 2015, **90**, 124–169.
23 L.-P. Peng, S. Nagarajan, S. Rasheed and C.-H. Zhou, *MedChemComm*, 2015, **6**, 222–229.
24 Z. Chen, M. J. Lee, R. Shahid Ashraf, Y. Gu, S. Albert-Seifried, M. Meedom Nielsen, B. Schroeder, T. D. Anthopoulos, M. Heeney, I. McCulloch and H. Sirringhaus, *Adv. Mater.*, 2012, **24**, 647–652.
25 J.-R. Pouliot, B. Sun, M. Leduc, A. Najari, Y. Li and M. Leclerc, *Polym. Chem.*, 2015, **6**, 278–282.
26 Z. Yi, S. Wang and Y. Liu, *Adv. Mater.*, 2015, **27**, 3589–3606.
27 J. Y. Back, H. Yu, I. Song, I. Kang, H. Ahn, T. J. Shin, S.-K. Kwon, J. H. Oh and Y.-H. Kim, *Chem. Mater.*, 2015, **27**, 1732–1739.
28 D. Khim, Y. R. Cheon, Y. Xu, W.-T. Park, S.-K. Kwon, Y.-Y. Noh and Y.-H. Kim, *Chem. Mater.*, 2016, **28**, 2287–2294.
29 H. Bronstein, Z. Chen, R. S. Ashraf, W. Zhang, J. Du, J. R. Durrant, P. Shakya Tuladhar, K. Song, S. E. Watkins, Y. Geerts, M. M. Wienk, R. A. J. Janssen, T. Anthopoulos, H. Sirringhaus, M. Heeney and I. McCulloch, *J. Am. Chem. Soc.*, 2011, **133**, 3272–3275.
30 I. Kang, H.-J. Yun, D. S. Chung, S.-K. Kwon and Y.-H. Kim, *J. Am. Chem. Soc.*, 2013, **135**, 14896–14899.
31 B. Sun, W. Hong, H. Aziz and Y. Li, *Polym. Chem.*, 2015, **6**, 938–945.
32 M. J. Frisch, *et al.*, *Gaussian 09 Revision D.01*, Gaussian, Inc., Wallingford, CT, USA, 2009. See ESI† for a full citation.
33 H. Yamagata and F. C. Spano, *J. Chem. Phys.*, 2012, **136**, 184901–184914.
34 R. Noriega, J. Rivnay, K. Vandewal, F. P. V. Koch, N. Stingelin, P. Smith, M. F. Toney and A. Salleo, *Nat. Mater.*, 2013, **12**, 1038–1044.
35 F. C. Spano and C. Silva, *Annu. Rev. Phys. Chem.*, 2014, **65**, 477–500.
36 J. Pommerehne, H. Vestweber, W. Guss, R. F. Mahrt, H. Bässler, M. Porsch, J. Daub, H. Bassler, M. Porsch and J. Daub, *Adv. Mater.*, 1995, **7**, 551–554.
37 G. Kim, S.-J. Kang, G. K. Dutta, Y.-K. Han, T. J. Shin, Y.-Y. Noh and C. Yang, *J. Am. Chem. Soc.*, 2014, **136**, 9477–9483.
38 S. Chen, B. Sun, W. Hong, H. Aziz, Y. Meng and Y. Li, *J. Mater. Chem. C*, 2014, **2**, 2183–2190.
39 D. M. de Leeuw, M. M. J. Simenon, A. R. Brown and R. E. F. Einerhand, *Synth. Met.*, 1997, **87**, 53–59.
40 T. D. Anthopoulos, G. C. Anyfantis, G. C. Papavassiliou and D. M. de Leeuw, *Appl. Phys. Lett.*, 2007, **90**, 122105.
41 H. T. Nicolai, M. Kuik, G. a. H. Wetzelaer, B. de Boer, C. Campbell, C. Risko, J. L. Brédas and P. W. M. Blom, *Nat. Mater.*, 2012, **11**, 882–887.
42 A. Virkar, S. Mannsfeld, J. H. Oh, M. F. Toney, Y. H. Tan, G. Liu, J. C. Scott, R. Miller and Z. Bao, *Adv. Funct. Mater.*, 2009, **19**, 1962–1970.
43 Y. Lei, B. Wu, W.-K. E. Chan, F. Zhu and B. S. Ong, *J. Mater. Chem. C*, 2015, **3**, 12267–12272.
44 B. Park, *Thin Solid Films*, 2015, **598**, 141–148.
45 X. Yan, H. Wang and D. Yan, *Thin Solid Films*, 2006, **515**, 2655–2658.
46 R. Schmidt, J. H. Oh, Y.-S. Sun, M. Deppisch, A.-M. Krause, K. Radacki, H. Braunschweig, M. Könemann, P. Erk, Z. Bao and F. Würthner, *J. Am. Chem. Soc.*, 2009, **131**, 6215–6228.
47 J. H. Oh, S. Suraru, W.-Y. Lee, M. Könemann, H. W. Höffken, C. Röger, R. Schmidt, Y. Chung, W.-C. Chen, F. Würthner and Z. Bao, *Adv. Funct. Mater.*, 2010, **20**, 2148–2156.
48 X. Guo, R. P. Ortiz, Y. Zheng, M.-G. Kim, S. Zhang, Y. Hu, G. Lu, A. Facchetti and T. J. Marks, *J. Am. Chem. Soc.*, 2011, **133**, 13685–13697.
49 T. Lei, Y. Cao, Y. Fan, C.-J. Liu, S.-C. Yuan and J. Pei, *J. Am. Chem. Soc.*, 2011, **133**, 6099–6101.
50 S. Lee, D. C. Borrelli and K. K. Gleason, *Org. Electron.*, 2016, **33**, 253–262.
51 L. Guo, J. Quinn, J. Wang, C. Guo, X. Li, J. Wang and Y. Li, *Dyes Pigm.*, 2016, **132**, 329–335.
52 G. Lu, H. Usta, C. Risko, L. Wang, A. Facchetti, M. A. Ratner and T. J. Marks, *J. Am. Chem. Soc.*, 2008, **130**, 7670–7685.

 

53 Y. Qiu, Y. Hu, G. Dong, L. Wang, J. Xie and Y. Ma, *Appl. Phys. Lett.*, 2003, **83**, 1644–1646.
54 Z.-T. Zhu, J. T. Mason, R. Dieckmann and G. G. Malliaras, *Appl. Phys. Lett.*, 2002, **81**, 4643–4645.
55 R. Ye, M. Baba, K. Suzuki, Y. Ohishi and K. Mori, *Thin Solid Films*, 2004, **464–465**, 437–440.
56 H. E. Gottlieb, V. Kotlyar and A. Nudelman, *J. Org. Chem.*, 1997, **62**, 7512–7515.
57 G. Horowitz, *Adv. Mater.*, 1998, **10**, 365–377.